Electronic Supplementary Information:

Vibrationally Induced Metallization of Energetic Azide αNaN$_3$

Adam A.L. Michalchuk, Svemir Rudić, Colin R. Pulham and Carole A. Morrison

Contents

S1 Vibrational frequencies for α-NaN$_3$

The zone-centre vibrational modes were calculated for crystalline α-NaN$_3$ using both the PBE-D2 and PBE-TS schemes, with resulting frequencies shown in Table S1.1.

Table S1.1: Zone centre vibrational frequencies for α-NaN$_3$ (primitive cell) based on the PBE DFT functional. Values are shown corresponding to the Grimme D2 (PBE-D2) and Tkatchenko-Scheffler (PBE-TS) dispersion corrections. LO-TO splitting is not considered.

	PBE-D2 /cm^{-1}	PBE-TS /cm^{-1}
M_1	150.974	126.970
M_2	177.998	174.320
M_3	202.210	187.008
M_4	214.510	189.240
M_5	220.220	226.954
M_6	606.277	611.254
M_7	609.716	612.105
M_8	1250.429	1252.237
M_9	1959.812	1961.848

S2 Inelastic Neutron Scattering Spectra for α-NaN$_3$

At low temperature, the intensity, *I*, of inelastic neutron scattering increases as[1]

$$I \propto (Q.u)^2$$

where Q is the momentum transfer and u is the total atomic displacement of the normal coordinate. On the TOSCA instrument, the back-scattering detectors follow a trajectory in $S(Q,\omega)$ slightly higher in Q than the forward scattering detectors.[2] Hence the intensity of the back-scattering detectors should exhibit larger scattering intensities. This is most notable at low wavenumber. However, for α-NaN$_3$, the low wavenumber scattering intensity is higher in the forward scattering detectors, Figure S1. This likely stems

from the dominant coherent scattering (directionally dependent) of NaN_3, and requires further investigation.

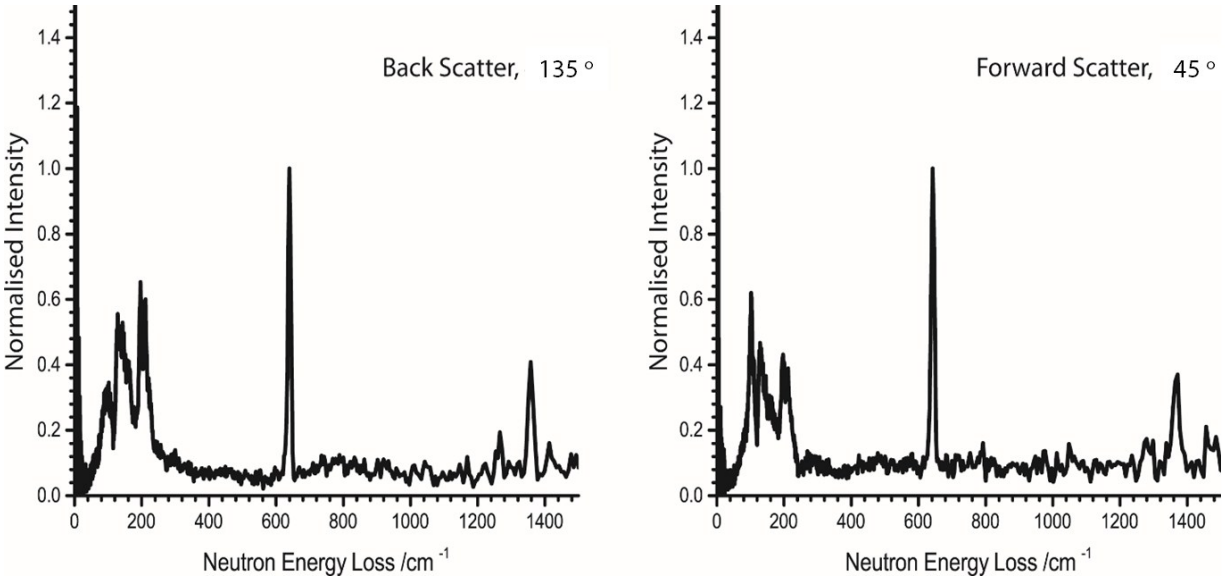

Figure S1: Inelastic neutron scattering spectra for α-NaN_3 at *ca* 20 K. Signal from the forward and back-scattering detectors are shown separately. Intensities have been normalised to the dominant peak at *ca* 630 cm^{-1}.

S3 Eigenvector 'walking' for M_{16} in α-NaN_3

The eigenvector associated with M_{16} exhibits considerable decrease in the band gap energy in α-NaN_3. Further extension of this eigenvector results in near metallisation, Figure S2.

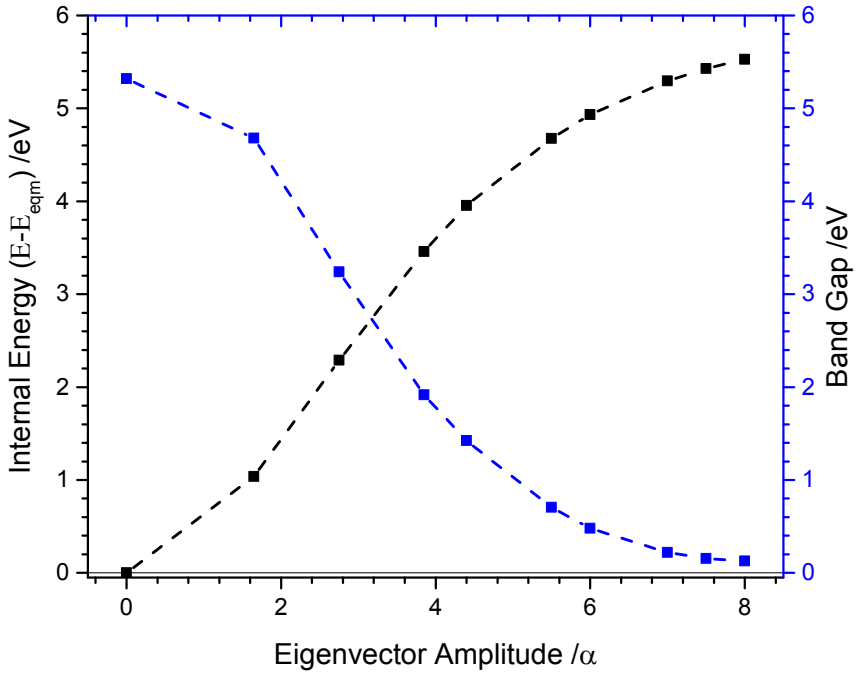

Figure S2: Band gap and internal energy along Mode 16, extended to $\alpha = 8$.

S4 Eigenvectors associated with the external modes of α-NaN_3

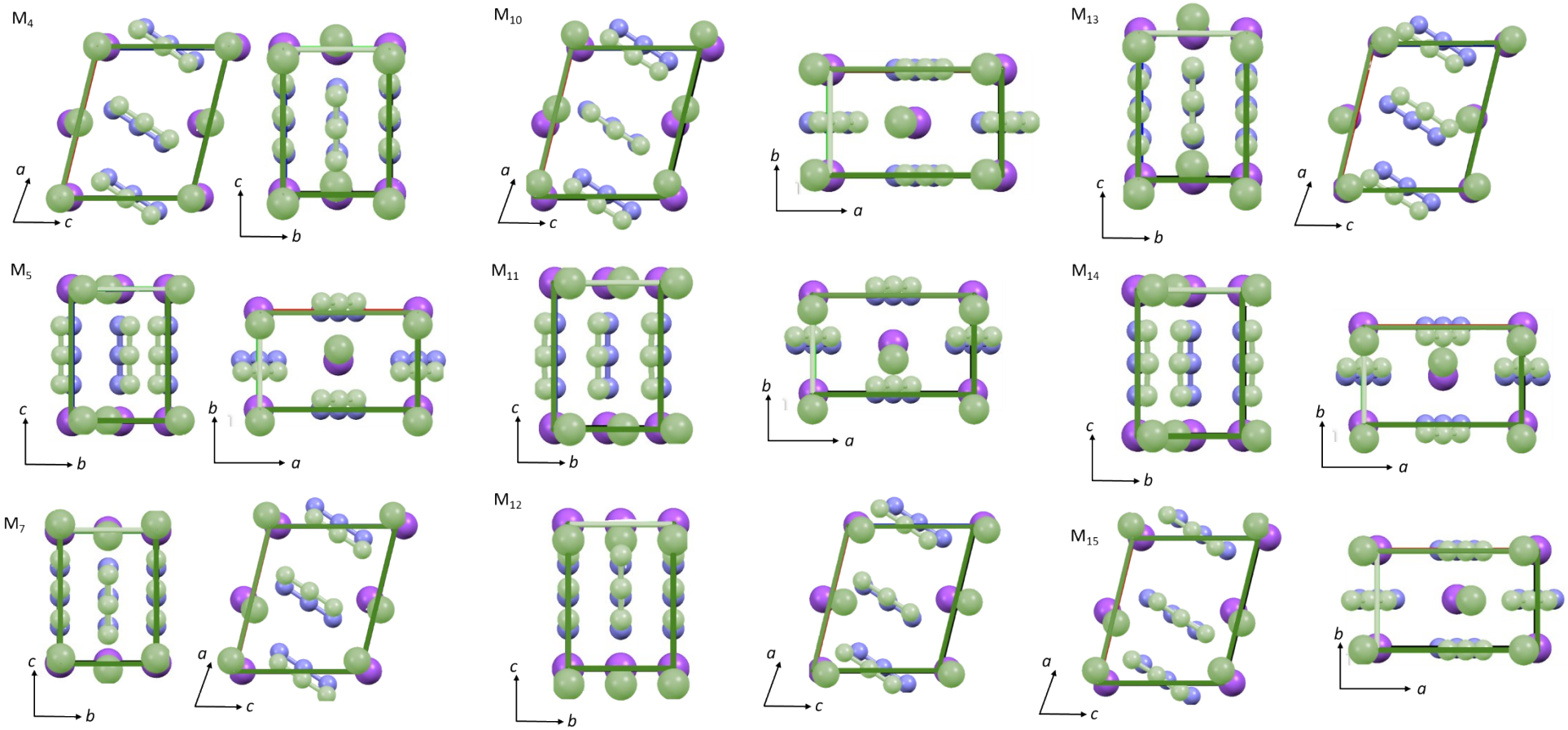

Figure S3: Eigenvectors of the external vibrational modes of α-NaN_3. Displacements are shown along the two crystallographic axes that best illustrate the distortion.

S5 Band Gap Reduction for M_{18}, M_{20}, M_{21} and M_{23}

The band gap was followed as a function of the eight internal modes of the conventional unit cell, Figure 6 and 8 in the main text, and Figure S4. Note that M_{21} is the out-of-phase symmetric stretching mode. As such, this mode could not be followed to metallisation due to compression of one of the azido anion molecules.

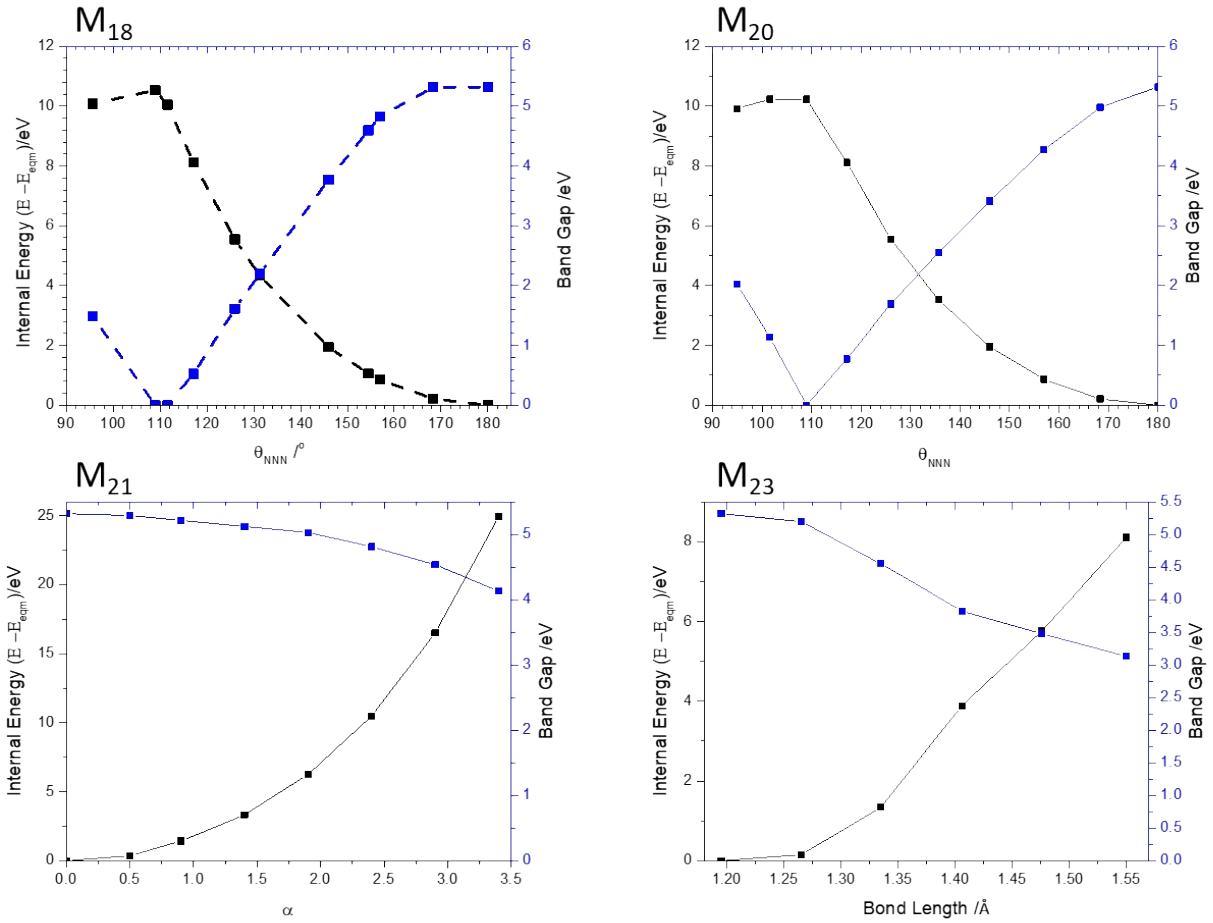

Figure S4: Band gap and internal energy as a function of the internal molecular modes of α-NaN_3.

S6 References

1 P. C. Mitchell, S. F. Parker, A. J. Ramirez-Cuesta and J. Tomkinson, *Vibrational Spectroscopy with Neutrons*, World Scientific, 2005.

2 D. Colognesi, M. Celli, F. Cilloco, R. J. Newport, S. F. Parker, V. Rossi-Albertini, F. Sacchetti, J. Tomkinson and M. Zoppi, *Appl. Phys. A Mater. Sci. Process.*, 2002, **74**, 64–66.